Journal of Biomechanics ∎ (∎∎∎∎) ∎∎∎–∎∎∎

Contents lists available at ScienceDirect

Journal of Biomechanics

journal homepage: www.elsevier.com/locate/jbiomech
www.JBiomech.com

A study of wall shear stress in 12 aneurysms with respect to different viscosity models and flow conditions

Øyvind Evju [a], Kristian Valen-Sendstad [a,b], Kent-André Mardal [a,*]

[a] Center for Biomedical Computing, Simula Research Laboratory, Martin Linges vei 17, Fornebu, Norway
[b] Biomedical Simulation Laboratory, Department of Mechanical & Industrial Engineering, University of Toronto, 5 Kings College Road, Toronto, ON, Canada

ARTICLE INFO

Article history:
Accepted 1 September 2013

Keywords:
Cerebral aneurysms
Computational fluid dynamics
Wall shear stress
Non-Newtonian fluid
Boundary conditions

ABSTRACT

Recent computational fluid dynamics (CFD) studies relate abnormal blood flow to rupture of cerebral aneurysms. However, it is still debated how to model blood flow with sufficient accuracy. Common assumptions made include Newtonian behaviour of blood, traction free outlet boundary conditions and inlet boundary conditions based on available literature. These assumptions are often required since the available patient specific data is usually restricted to the geometry of the aneurysm and the surrounding vasculature. However, the consequences of these assumptions have so far been inadequately addressed.

This study investigates the effects of 4 different viscosity models, 2 different inflow conditions and 2 different outflow conditions in 12 middle cerebral artery aneurysms. The differences are quantified in terms of 3 different wall shear stress (WSS) metrics, involving maximal WSS, average WSS, and proportion of aneurysm sac area with low WSS. The results were compared with common geometrical metrics such as volume, aspect ratio, size ratio and parent vessel diameter and classifications in terms of sex and aneurysm type.

The results demonstrate strong correlations between the different viscosity models and boundary conditions. The correlation between the different WSS metrics range from weak to medium. No strong correlations were found between the different WSS metrics and the geometrical metrics or classifications.

© 2013 Elsevier Ltd. All rights reserved.

1. Introduction

Cerebral aneurysms are relatively common. Around 1–6% of the population develop aneurysms during a life-time (Schievink, 1997) and often at a quite early age (50–60 years). The rupture of a cerebral aneurysm causes subarachnoid hemorrhage (SAH), a stroke associated with high risk of morbidity, and a mortality rate as high as 60% within 30 days (le Roux and Wallace, 2010). The rupture risk is however quite low, usually estimated to less than 1% per year (Rinkel et al., 1998). Risk of rupture has been related to the size and morphology of aneurysms and their surrounding vasculature, but individual risk assessment is still not feasible. CFD could potentially aid clinicians in individualized assessment and treatment planning, and is therefore under active research.

Recently, three large retrospective computational studies have demonstrated that fluid dynamics simulations can be used to discriminate ruptured from non-ruptured aneurysms (Cebral et al., 2011a, 2011b; Xiang et al., 2011). However, what constitutes an appropriate computational model is an open question. Fluid–structure interaction (e.g. Bazilevs et al., 2010; Isaksen et al., 2008) and non-linear viscosity models (e.g. Gambaruto et al., 2011; Xiang et al., 2012) have received some attention as extensions of the more commonly used Newtonian flow simulations within rigid vessels. Still, while these studies argue for adding complexity to the model, they typically employ relatively simple boundary conditions obtained from the literature and only consider a few aneurysms.

Vascular remodelling due to flow conditions was observed already 150 years ago by Virchow. As demonstrated more recently by e.g. Chien (2007) and Hoi et al. (2008), among others, the wall shear stress (WSS) acting on the endothelial cells surfacing the arterial wall plays a central role in this remodelling. It has been shown that aneurysms grow in the direction of low WSS (Boussel et al., 2008), but there is no conclusion whether low or high WSS correlates with rupture status. That is, certain studies have found high WSS to be correlated with rupture status (Jou et al., 2008; Cebral et al., 2011b), which contrasts the correlation of low WSS reported by others (Xiang et al., 2011; Miura et al., 2013).

Recently, clinical researchers have expressed scepticism towards CFD analysis because of the overwhelming and confounding number of models and flow metrics, c.f. the editorial in AJNR (Kallmes, 2012). It is therefore timely to compare different models and metrics in an effort to reduce this number. In this study we simulate flow in 12

* Correspondence to: Center for Biomedical Computing, Simula Research Laboratory, P.O. Box 134, N-1325 Lysaker, Norway. Tel.: +47 93610854.
E-mail address: kent-and@simula.no (K.-A. Mardal).

0021-9290/$ - see front matter © 2013 Elsevier Ltd. All rights reserved.
http://dx.doi.org/10.1016/j.jbiomech.2013.09.004

different middle cerebral artery (MCA) aneurysms, 4 different viscosity models, 2 different inflow boundary conditions and 2 different outflow boundary conditions. We included natural sex and age variations in the hematocrit levels of the viscosity models. WSS is quantified in terms of three different metrics: maximal WSS, average WSS, and proportion of aneurysm sac area with low WSS with respect to the different viscosity models and boundary conditions. We also compare with common geometry metrics such as aneurysm volume, aspect ratio, and parent vessel diameter and classifications in terms of sex and aneurysm type.

2. Methods

Computed tomography angiography (CTA) volume images were obtained from a 16 multi-detector row spiral scanner (Somatom Sensation 16; Siemens, Erlangen, Germany) taken from 12 MCA aneurysms treated at the Department of Neurosurgery, University Hospital of North Norway between 2006 and 2008. The register was approved by the local ethics committee and data inspectorate.

The Vascular Modelling Toolkit (VMTK) was used to segment the CTA images and create CFD meshes. The aneurysm models have been meshed with 800,000–1,200,000 tetrahedral cells containing three boundary layers. The isolation of the aneurysm sac was done using the same approach as Ford et al. (2009). We used a previously developed and validated Navier–Stokes solver (Valen-Sendstad et al., 2012a) implemented in FEniCS (Logg et al., 2011), with minor extensions to stabilize the flow for larger time steps. Specifically, we implemented an incremental pressure correction scheme (Goda, 1979) with semi-implicit handling of the nonlinear convection term, implicit Euler time-stepping and used first order linear continuous elements for both the velocity and pressure. This scheme was found favorable when compared to the schemes in Valen-Sendstad et al. (2012a) in terms of the accuracy and efficiency. A thorough comparison and verification of this scheme can be found in Evju (2011), which shows that the scheme is second order accurate in space and first order in time.

Mesh convergence for the involving meshes has been verified in a previous study (Valen-Sendstad, 2011, paper IV), where the maximal pointwise kinetic energy and total kinetic energy varied with less than 2% between the two finest meshes for all cases, and the maximal pointwise vorticity and integrated vorticity varied with less than 5% between the same meshes. A time step of 1.25 ms was used, which gave 800 time steps per second. The simulations were run for four cycles to eliminate cyclic variations, and the solution was saved at every fifth time step of the fourth cycle.

For all the 12 aneurysm geometries (see Fig. 1), we employed and compared four different viscosity models, two different inlet boundary conditions and two different outlet boundary conditions, for a total of 72 simulations. The different viscosity models are summarized in Table 1. A Newtonian viscosity model with a value of 0.00345 Pa s was used as reference. The Casson model incorporates hematocrit and asymptotic viscosity. Hematocrit level varies according to age and sex and we have chosen hematocrit levels 38% (C38) and 40% (C40) corresponding to women before and after menopause (Jacobsen et al., 2012). The shear-rate dependence of all viscosity models is as visualized in Fig. 2. The marked area in this figure demonstrates the asymptotic behaviour of the different viscosity models, ranging from shear rates typical for healthy MCAs. The Newtonian reference model has the same viscosity as the asymptotic value of the modified Cross model, making this model relevant for isolating the shear thinning effects. Both the Casson models have lower asymptotic values, and the difference between them reflects the change in hematocrit.

The inlet velocity is set to be a linear interpolation of a parabolic profile radially in space. The spatial peak velocity is determined by using a pulsatile waveform, depicted in Fig. 3. This waveform is taken from the MCA segment of a female patient undergoing cerebrovascular treatment. For our reference calculations, the spatial peak velocity has been scaled to a timed average of 0.75 m/s, which has been found to be an average flow velocity in female MCAs (Krejza et al., 2005). As a comparison to this, we have also employed a set of simulations using a reduced inflow velocity of 25% to 0.56 m/s, roughly corresponding to the average velocity in the MCA of people aged >60. For all simulations we used a heart rate of 75 beats per minute, and a density of 1056 kg/m^3.

To represent the peripheral resistance, a resistance condition is applied at the outlets in the reference simulations:

$$p = CQ_o,$$

where Q_o is the flow rate though the outlet. The value of the coefficient is set to $C = 5.97 \times 10^9$ Pa s/m^3 for the MCA (Alastruey et al., 2007). The traction free outflow conditions corresponds to $C=0$. The parameters used for each set of simulations have been summarized in Table 2.

For the reference case, we computed some key flow properties, shown in Table 3. The Reynolds number (Re) is computed as $QD/(\nu A)$, where Q, D, ν, and A are the inlet flow rate, parent vessel diameter, kinematic viscosity, and parent vessel cross sectional area, respectively. The Womersley number (Wo) is computed as $R(\omega/\nu)^{1/2}$, where R is the radius and ω is the angular frequency. The inlet WSS (IWSS) is calculated from the Poiseuille formula, $\tau = 8\mu Q/(DA)$, where μ corresponds to the Newtonian viscosity value. The inlet diameter varies from 1.5 mm to 3.5 mm, roughly a factor 2.3, which is also reflected in the Reynolds and Womersley numbers. Correspondingly, the flow rate varies by a factor of 5.2, or 2.3^2, from 0.633 mL/s to 3.600 mL/s. The IWSS is inversely related to the diameter.

The WSS magnitude has been time-averaged over the full cardiac cycle, and normalized with the IWSS. Based on results of previous studies on the relationship between WSS and aneurysm growth and rupture (see for example Cebral et al., 2011b; Xiang et al., 2011; Jou et al., 2008), we have chosen and calculated three WSS metrics. These are the maximum WSS of the aneurysm sac (MWSS), the average WSS over the aneurysm sac (AWSS) and the area of low shear (LSA) which have been defined as the area where the normalized WSS is less than 0.1, divided by the total sac area.

The correlation was calculated using Pearson's correlation coefficient. With two sets of measurements $X = \{x_1, x_2, \ldots, x_n\}$ and $Y = \{y_1, y_2, \ldots, y_n\}$, the coefficient is calculated as

$$r_{X,Y} = \frac{\sum_{i=1}^{n}(x_i - \bar{x})(y_i - \bar{y})}{\sqrt{\sum_{i=1}^{n}(x_i - \bar{x})^2 \sum_{i=1}^{n}(y_i - \bar{y})^2}}$$

where $\bar{x}$ and $\bar{y}$ is the sample mean of X and Y, respectively. Strong, medium, and weak correlation are defined by absolute values of $r_{X,Y}$ greater than 0.8, greater than 0.4, and less than 0.4, respectively. For the data with binary outcome, sex and aneurysm type, we let men and bifurcation take the value 1, while women and sidewall are 0.

3. Results

Average WSS: There are large differences in AWSS between the aneurysms in the reference case, ranging from a minimum value of 0.24 (A12) to a maximum of 1.8 (A6) (ratio 7.7), with an average value of 0.94, as shown in Fig. 4a. The effects of the different viscosity models differ from the reference in the range -9.4% to 5.3%. The variations are largest for the C38 case, with an average decrease of 3.1% and a standard deviation of 3.8%. The modified Cross model, which is the only model that isolates the shear thinning, predicts the smallest deviations on an average (0.5%) and has the lowest standard deviation (2.4%).

For the cases with modified boundary conditions, we see that the differences from the reference are far larger than in the non-Newtonian cases. For the reduced inflow case, the AWSS was significantly reduced on an average (-22.4%). This suggests that the WSS in the aneurysm is more sensitive to flow changes than what a linear relationship would predict.

For the traction free case, the results vary greatly, from -6.8% to 36.1%. It is worth noting that the three traction free simulations causing the largest differences from the reference simulations are A1, A4 and A5, where the aneurysms all occur downstream from a modelled bifurcation, see also Fig. 1. The different outflow conditions do in these cases cause a significantly different flow diversion between the different outlets (A1: 36.1%, A4: -6.8%, and A5: 12.4%) and correspondingly different flow and WSS within the aneurysms. For the other aneurysms, the changes are of the same order as for the non-Newtonian cases.

Maximum WSS: As shown in Fig. 4b, the MWSS reference values vary from 2.3 (A11) to 11 (A9) (ratio 4.6), with an average value of 6.0. The changes caused by the viscosity models range from -7.7% to 3.9%. Again, the C38 model yields the greatest variations, with a standard deviation of 3.5%. Similar results are obtained for the C40 case. The modified Cross model is again the most coherent with the reference values, although a clear indication is shown for a slightly lower MWSS, with an average decrease of 2.8% and standard deviation of 2.0%.

We also note that the viscosity seems to be of greater significance in some aneurysms than others. In aneurysm A4 for example, the C38 model predicts an increase as high of 3.9%, the C40 model predicts an increase of 2.2% and the MC model predicts a -7.2% change. In other aneurysms, such as A2 and A3, the MWSS seems to be much less dependent on viscosity.

Please cite this article as: Evju, Øyvind, et al., A study of wall shear stress in 12 aneurysms with respect to different viscosity models and flow conditions. Journal of Biomechanics (2013), http://dx.doi.org/10.1016/j.jbiomech.2013.09.004

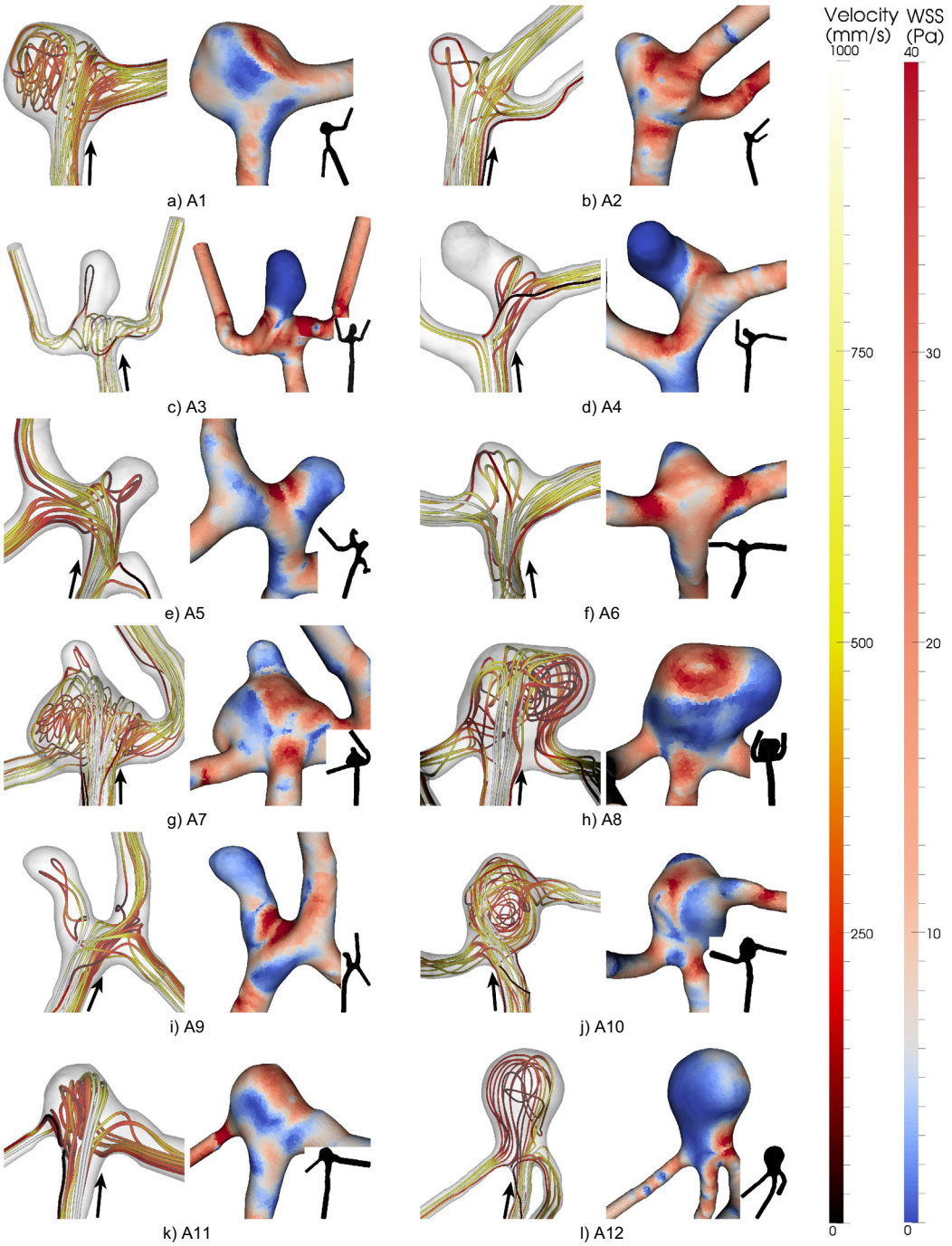

Fig. 1. The 12 different aneurysms used in simulations. Streamlines of the velocity at systole on the left, and the corresponding WSS magnitude on the right. The inflow is from below. Images are created from the reference simulations.

For the reduced inflow case, we see very similar variations as found for AWSS. Again, the average decrease in MWSS is more sensitive than the 25% reduction predicted by linear relationship, with an average additional decrease of 22.9%. The variations for the traction free case are large, ranging from −4.0% to 37.4%. The results are not coherent with those for the AWSS. In aneurysm A6 for example, we see an increase in max WSS of 16.9%. This is in contrast to the results for AWSS, which showed an increase of only 1.5%. In this particular case, the MWSS occurs close to the edge of the isolated aneurysm sac causing this peak WSS to fall outside the sac in the case in the reference simulation.

Area of low WSS: For the LSA metric, the reference values vary greatly, from 0.002 (A1) to 0.59 (A4) (ratio 293), and the average is 0.17, as seen in Fig. 4c. There are mainly three aneurysms (A3, A4 and A12) that contribute to the relatively high average area.

The shear thinning effects, isolated in the modified Cross model, tend towards a reduced LSA. The two Casson models predict similar changes. Overall, there are only small variations caused by the viscosity models, with differences in the range −0.037 to 0.022.

The reduced inflow case shows the largest changes by far, with an average increase of 0.046. In all aneurysms, this case predicted an increased area, however, the variations between the aneurysms are large. Case A5 is particularly interesting, as this increases to 0.233, almost three times the reference value.

Please cite this article as: Evju, Øyvind, et al., A study of wall shear stress in 12 aneurysms with respect to different viscosity models and flow conditions. Journal of Biomechanics (2013), http://dx.doi.org/10.1016/j.jbiomech.2013.09.004

Table 1
The viscosity models used in the simulations. The modified Cross and Casson model parameters are taken from Robertson et al. (2009) and Yeow et al. (2002), Dintenfass (1985), respectively.

Name	Model	Parameters
Newtonian	$\mu = 0.00345$ Pa s	
Modified Cross	$\hat{\mu} = (1+(\lambda\dot{\gamma})^m)^{-a}$	$\hat{\mu} = (\mu-\mu_\infty)/(\mu_0-\mu_\infty)$, $\lambda = 3.736$ s, ; $m = 2.406$, $a = 0.254, \mu_0 = 0.056$ Pa s, $\mu_\infty = 0.00345$ Pa s
Casson	$\mu = \frac{\tau_y}{\dot{\gamma}} + \frac{2\sqrt{\mu_\infty}\sqrt{\tau_y}}{\sqrt{\dot{\gamma}}} + \mu_\infty$	$\tau_y = 0.02687\ H^3$ Pa s, $\mu_\infty = \eta_0(1-TkH)^{-2.5}$, $\eta_0 = 0.00145$ Pa s, $Tk = 0.62$, (H = Hematocrit).

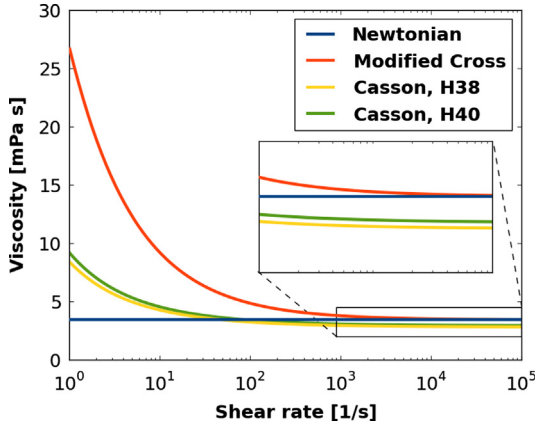

Fig. 2. The viscosity as a function of the shear rate for the different viscosity models.

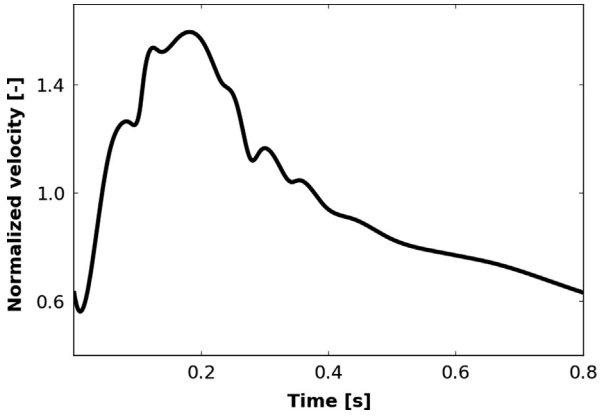

Fig. 3. Normalized waveform.

Table 2
A summary of the parameters used in the different simulations. The simulations described by the first row is used as a reference for the comparisons with the other simulations.

Simulation	Key	Viscosity	Inflow condition	Outflow condition
Reference	Ref.	Newtonian	0.75 m/s	Resistance
Modified Cross	MC	Modified Cross	Ref.	Ref.
Casson, H40	C40	Casson, hct 40%	Ref.	Ref.
Casson, H38	C38	Casson, hct 38%	Ref.	Ref.
Traction free	TF	Ref.	Ref.	Traction free
Reduced inflow	RI	Ref.	0.56 m/s	Ref.

Table 3
A summary of the reference simulations, with inlet diameter, Reynolds and Womersley numbers, flow rate, calculated average WSS at the inlet, rupture status (ruptured/unruptured), type (sidewall/bifurcation), sex, aneurysm volume, aspect ratio and size ratio.

Aneurysm	D (mm)	Re (–)	Wo (–)	Q (mL/s)	IWSS (Pa)	Status	Type	Sex	V (mm^3)	AR (–)	SR (–)
A1	3.43	386	2.66	3.40	2.96	U	S	M	212	1.15	3.04
A2	2.51	248	1.95	1.59	3.54	U	B	F	33	0.90	1.59
A3	2.49	241	1.93	1.54	3.49	R	B	F	54	1.80	3.61
A4	2.12	222	1.64	1.21	4.45	U	S	F	43	1.42	3.08
A5	1.96	209	1.52	1.05	4.92	U	S	F	13	1.08	1.54
A6	2.55	282	1.98	1.85	3.91	R	B	M	18	0.79	1.58
A7	3.53	398	2.74	3.60	2.88	R	B	M	509	1.00	3.95
A8	2.40	264	1.86	1.62	4.14	R	B	F	278	0.94	3.86
A9	2.24	246	1.74	1.42	4.41	R	S	F	33	2.10	3.74
A10	2.68	298	2.08	2.05	3.74	R	B	F	265	0.80	3.32
A11	1.55	159	1.20	0.63	6.00	R	B	F	24	0.59	1.65
A12	1.74	184	1.35	0.82	5.46	U	B	M	251	2.25	5.85

The traction free case displays only minor changes, comparable to the changes caused by different viscosity models. The differences range from −0.012 to 0.028.

Correlation: Shown in Fig. 5 are scatterplots of each metric, comparing the values from the reference case with those obtained by the other cases. The linear correlation is very strong for all cases, with r-values of 0.95 or higher. The differences in viscosity models give correlation values of 0.995 or higher.

Table 4 shows the correlation matrix between aneurysm type, sex, parent vessel diameter (D), aneurysm volume (V), aspect ratio (AR), size ratio (SR), MWSS, AWSS, and LSA. There are no strong correlations, but there are medium correlations between LSA and AR (0.72), SR and AR (0.71), AWSS and LSA (−0.63), SR and V (0.60), D and V (0.59), AWSS and AE (0.52), LSA and SE (0.50), D and Sex (0.47), Sex and V (0.48), and Sex and AWSS (0.44). The rest of the correlations are low. Fig. 6 shows the relationship between the different WSS metrics.

4. Discussion

This study investigates 3 different WSS metrics in 12 cerebral aneurysms with respect to 2 different inflow conditions, 2 different outflow conditions, and 4 different viscosity models. The different WSS metrics showed only weak or medium correlation (−0.06, 0.40 and −0.63) between each other and the other geometrical metrics. The different viscosity models gave less than 4% change on an average for the different WSS metrics. Furthermore, the different viscosity models and boundary conditions all showed strong correlation (>0.95).

The low sensitivity of average WSS with respect to the viscosity model is consistent with other studies (Gambaruto et al., 2011; Jiang et al., 2011; Lee and Steinman, 2007), which concern one single cerebral aneurysm, a canine model aneurysm, and carotid arteries. Furthermore, neglecting the non-Newtonian effects of blood may underestimate the average WSS, as well as overestimate the maximum WSS, which is coherent with the recent study (Chen and Lu, 2006).

We have investigated 4 different viscosity models, but many other nonlinear viscosity models have been proposed or considered (see for example Gambaruto et al., 2011; Chen and Lu, 2006). However, during this study, we considered seven different viscosity models initially, and similar results were obtained with all models (Evju, 2011).

Please cite this article as: Evju, Øyvind, et al., A study of wall shear stress in 12 aneurysms with respect to different viscosity models and flow conditions. Journal of Biomechanics (2013), http://dx.doi.org/10.1016/j.jbiomech.2013.09.004

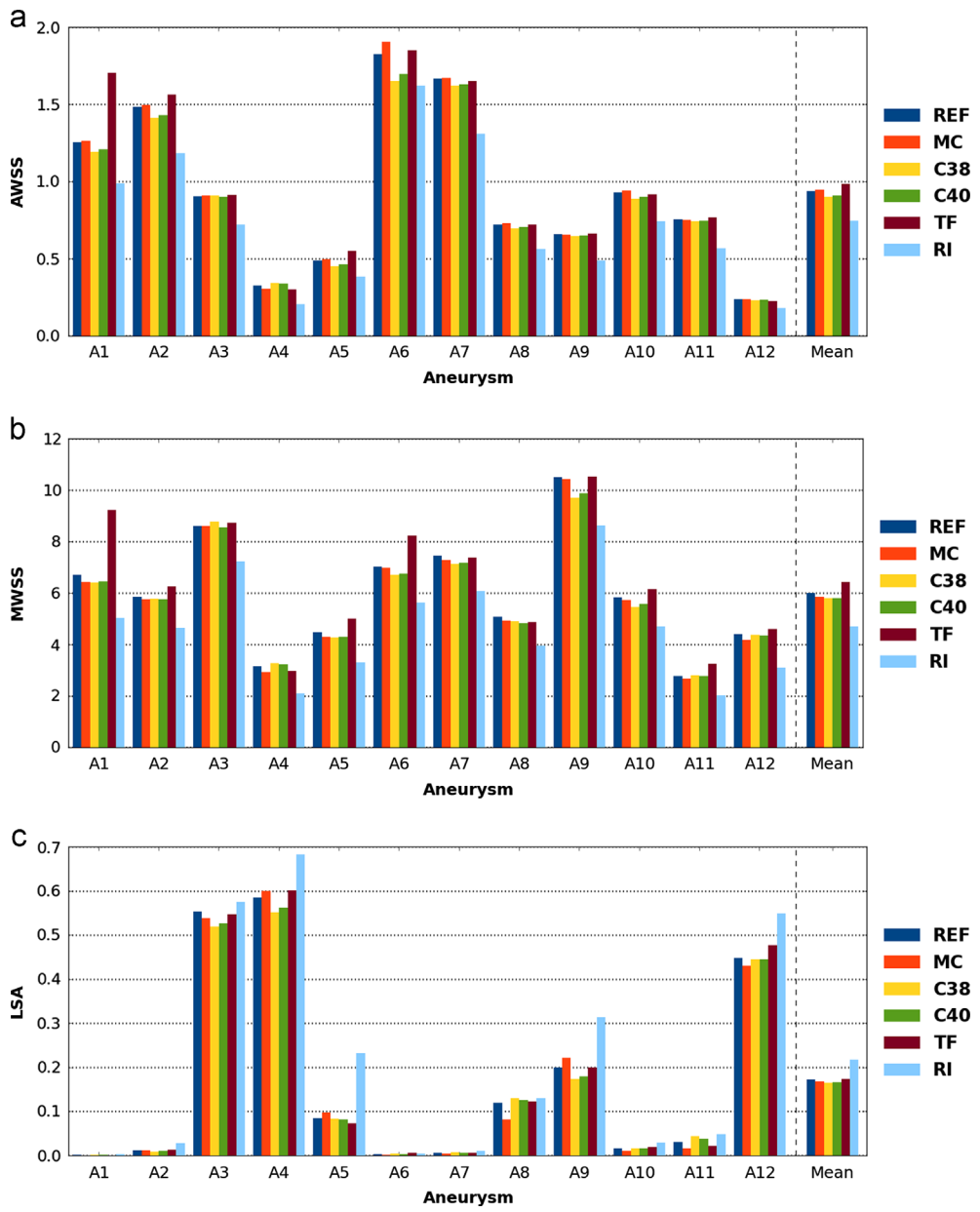

Fig. 4. The different WSS metrics for the different aneurysms, viscosity models and boundary conditions. From top to bottom, the AWSS, MWSS, and LSA values are displayed.

We have assumed the vessel and aneurysm walls to be rigid and impermeable, which is reasonable for flow and WSS prediction in finite segments of large arteries (Steinman, 2012). Furthermore, we have implicitly used the common assumption that the flow is laminar through the choice of the numerical solver and resolution in both time and space, although this assumption has recently been challenged (Valen-Sendstad et al., 2011). Removing these simplifications would require additional patient-specific parameters to be determined and cause a significant increase in computational time. In addition, these chosen simplifications are the most common in clinical studies.

The hematocrit levels vary with age and sex (Jacobsen et al., 2012), with a clear increase in women with increasing age. Women also have increased risk of rupture (Linn et al., 1996; de Rooij et al., 2007) and it is natural to question whether these natural viscosity variations can alter the WSS significantly and perhaps help explain the increased rupture risk. However, as we have seen in this study, the differences in WSS in MCA aneurysms caused by the different viscosity models are relatively small compared to the WSS variations among the different individuals. The sex differences in rupture risk may be related to the fact that women on an average have vessels with smaller diameters than men (Lindekleiv et al., 2010). We found a medium correlation between sex and vessel diameter and aneurysms volume.

The recent works (Baharoglu et al., 2012; Valen-Sendstad et al., 2012b) suggest that the flow differs in bifurcation and sidewall aneurysms. However, in our current study, there are only weak correlations between the aneurysm type and the different metrics.

Recently, clinical researchers have expressed scepticism towards CFD analysis despite years of enthusiasm. The scepticism arose mainly because of the overwhelming number of models and flow characterizations described in a rapidly growing number of papers on the topic, c.f. e.g. the editorial in AJNR (Kallmes, 2012) and its response from CFD practitioners (Robertson and Watton, 2012;

Please cite this article as: Evju, Øyvind, et al., A study of wall shear stress in 12 aneurysms with respect to different viscosity models and flow conditions. Journal of Biomechanics (2013), http://dx.doi.org/10.1016/j.jbiomech.2013.09.004

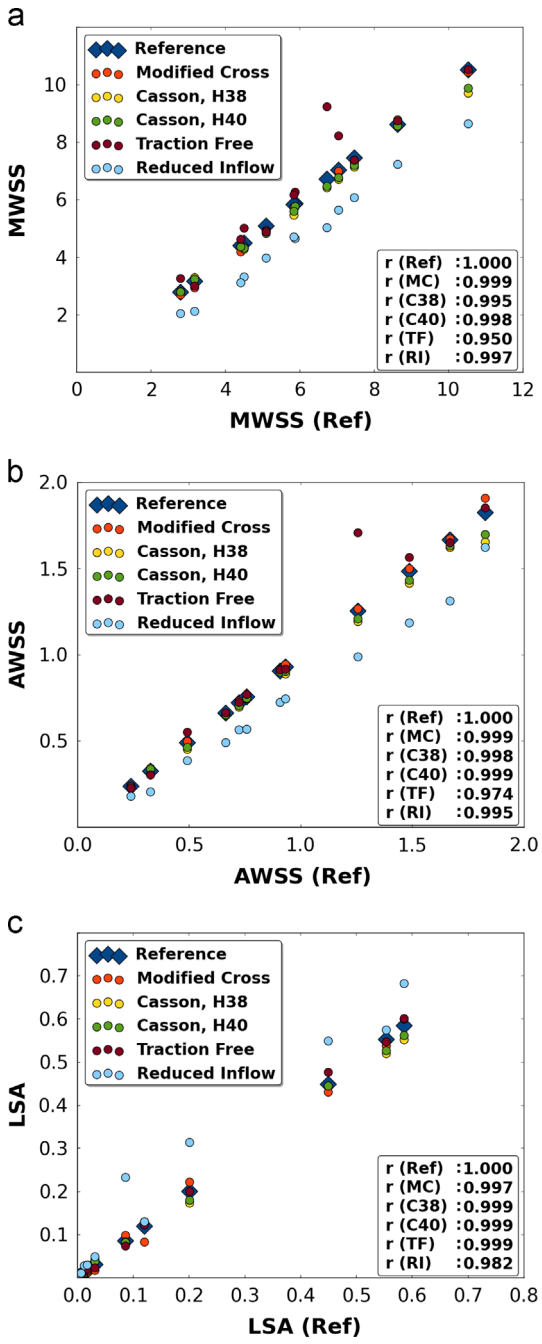

Fig. 5. Scatterplots of each metric, comparing the values from the reference case with those obtained by the other cases.

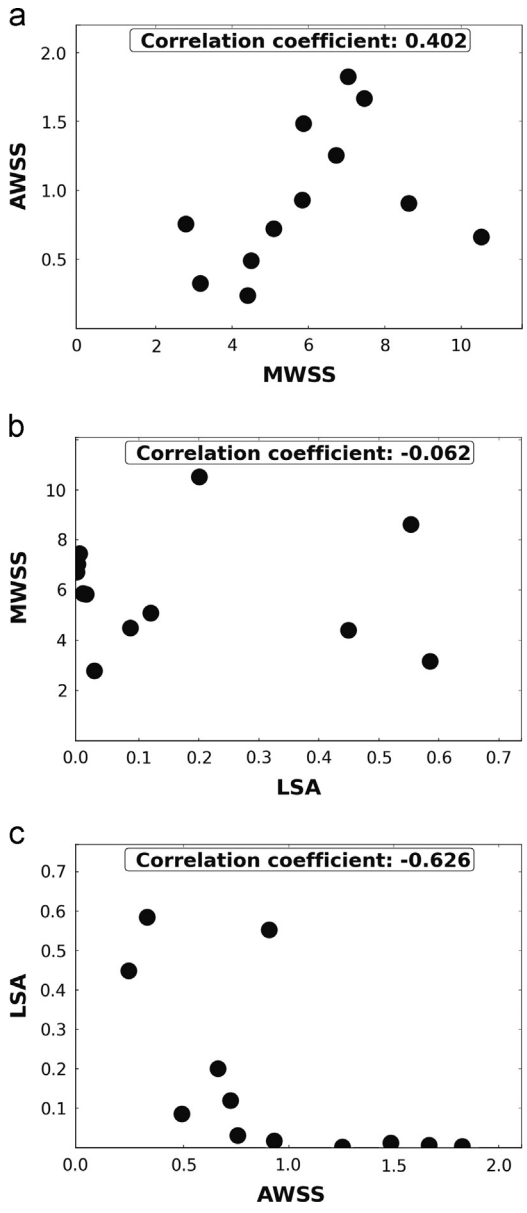

Fig. 6. Scatterplots of the different WSS metrics for the references simulations.

Table 4
Correlations between parent vessel diameter, aneurysm type, sex, aneurysm volume, aspect ratio, size ratio, MWSS, AWSS, and LSA for the reference simulations.

	D	Type	Sex	V	AR	SR	MWSS	AWSS	LSA
D	1.00	0.01	0.47	0.59	−0.21	0.08	0.50	0.70	−0.38
Type		1.00	−0.13	−0.32	0.28	−0.12	0.07	−0.36	0.15
Sex			1.00	0.48	0.09	0.30	0.13	0.44	−0.19
V				1.00	−0.05	0.60	0.07	0.21	−0.21
AR					1.00	0.71	0.38	−0.52	0.72
SR						1.00	0.19	−0.39	0.50
MWSS							1.00	0.40	−0.06
AWSS								1.00	−0.63
LSA									1.00

Cebral and Meng, 2012). Based on our study, different WSS metrics do not have strong correlation and it is therefore important to find the right WSS metrics. On the other hand, the different viscosity models and boundary conditions correlate strongly.

5. Conclusion

This study shows that the different viscosity models and boundary conditions correlate strongly for three different WSS metrics. The correlation between the different WSS metrics ranges from weak to medium. No strong correlations were found between the different WSS metrics and the geometrical metrics or classifications.

Conflict of interest statement

All authors declare that there are no conflicts of interest.

Please cite this article as: Evju, Øyvind, et al., A study of wall shear stress in 12 aneurysms with respect to different viscosity models and flow conditions. Journal of Biomechanics (2013), http://dx.doi.org/10.1016/j.jbiomech.2013.09.004

ARTICLE IN PRESS

Acknowledgements

This work has been supported by Research Council of Norway through grant no. 209951 and a Center of Excellence grant awarded to the Center for Biomedical Computing at Simula Research Laboratory.

References

Alastruey, J., Parker, K., Peiro, J., Byrd, S., Sherwin, S., 2007. Modelling the Circle of Willis to assess the effects of anatomical variations and occlusions on cerebral flows. Journal of Biomechanics 40, 1794–1805.

Baharoglu, M.I., Lauric, A., Gao, B.L., Malek, A.M., 2012. Identification of a dichotomy in morphological predictors of rupture status between sidewall-and bifurcation-type intracranial aneurysms. Journal of Neurosurgery 116, 871–881.

Bazilevs, Y., Hsu, M.C., Zhang, Y., Wang, W., Kvamsdal, T., Hentschel, S., Isaksen, J., 2010. Computational vascular fluid–structure interaction: methodology and application to cerebral aneurysms. Biomechanics and Modeling in Mechanobiology 9, 481–498.

Boussel, L., Rayz, V., McCulloch, C., Martin, A., Acevedo-Bolton, G., Lawton, M., Smith, R.H.W.S., Young, W.L., Saloner, D., 2008. Aneurysm growth occurs at region of low wall shear stress: patient-specific correlation of hemodynamics and growth in a longitudinal study. Stroke 39, 2997–3002.

Cebral, J., Meng, H., 2012. Counterpoint: realizing the clinical utility of computational fluid dynamics—closing the gap. American Journal of Neuroradiology 33, 396–398.

Cebral, J., Mut, F., Weir, J., Putman, C., 2011a. Association of hemodynamic characteristics and cerebral aneurysm rupture. American Journal of Neuroradiology 32, 264–270.

Cebral, J., Mut, F., Weir, J., Putman, C., 2011b. Quantitative characterization of the hemodynamic environment in ruptured and unruptured brain aneurysms. American Journal of Neuroradiology 32, 145–151.

Chen, J., Lu, X.Y., 2006. Numerical investigation of the non-Newtonian pulsatile blood flow in a bifurcation model with a non-planar branch. Journal of Biomechanics 39, 818–832.

Chien, S., 2007. Mechanotransduction and endothelial cell homeostasis: the wisdom of the cell. American Journal of Physiology – Heart and Circulatory Physiology 292, 1209–1224.

Dintenfass, L., 1985. Red cell rigidity, Tk, and filtration. Clinical Hemorheology 5, 241–244.

Evju, Ø., 2011. Sensitivity Analysis of Simulated Blood Flow in Cerebral Aneurysms. Master's Thesis. DUO, University of Oslo.

Ford, M., Hoi, Y., Piccinelli, M., Antiga, L., Steinman, D.A., 2009. An objective approach to digital removal of saccular aneurysms: technique and applications. British Journal of Radiology 82, 55–61.

Gambaruto, A.M., Janela, J., Moura, A., Sequeira, A., 2011. Sensitivity of hemodynamics in a patient specific cerebral aneurysm to vascular geometry and blood rheology. Mathematical Biosciences and Engineering 8, 409–423.

Goda, K., 1979. A multistep technique with implicit difference schemes for calculating two- or three-dimensional cavity flows. Journal of Computational Physics 30, 76–95.

Hoi, Y., Gao, L., Tremmel, M., Paluch, R., Siddiqui, A., Meng, H., Mocco, J., 2008. In vivo assessment of rapid cerebrovascular morphological adaptation following acute blood flow increase. Journal of Neurosurgery 109, 1141–1147.

Isaksen, J.G., Bazilevs, Y., Kvamsdal, T., Zhang, Y., Kaspersen, J.H., Waterloo, K., Romner, B., Ingebrigtsen, T., 2008. Determination of wall tension in cerebral artery aneurysms by numerical simulation. Stroke 39, 3172–3178.

Jacobsen, B.K., Eggen, A.E., Mathiesen, E.B., Wilsgaard, T., Njølstad, I., 2012. Cohort profile: the Tromsø study. International Journal of Epidemiology 41, 961–967.

Jiang, J., Johnson, K., Valen-Sendstad, K., Mardal, K.A., Wieben, O., Strother, C., 2011. Flow characteristics in a canine aneurysm model: a comparison of 4-D accelerated phase-contrast MR measurements and computational fluid dynamics simulations. Medical Physics 38, 6300–6313.

Jou, L., Lee, D., Morsi, H., Mawad, M., 2008. Wall shear stress on ruptured and unruptured intracranial aneurysms at the internal carotid artery. American Journal of Neuroradiology 29, 1761–1767.

Kallmes, D., 2012. Point CFD—computational fluid dynamics or confounding factor dissemination. American Journal of Neuroradiology 33, 395–396.

Krejza, J., Szydlik, P., Liebeskind, D.S., Kochanowicz, J., et al., 2005. Age and sex variability and normal reference values for the VMCA/VICA index. American Journal of Neuroradiology 26, 730–735.

Lee, S.W., Steinman, D.A., 2007. On the relative importance of rheology for image-based CFD models of the carotid bifurcation. Journal of Biomechanical Engineering 129, 273–278.

Lindekleiv, H.M., Valen-Sendstad, K., Morgan, M.K., Mardal, K.A., et al., 2010. Sex differences in intracranial arterial bifurcations. Gender Medicine 7, 149–155.

Linn, F., Rinkel, G., Algra, A., van Gijn, J., 1996. Incidence of subarachnoid hemorrhage: role of region, year, and rate of computed tomography: a meta-analysis. Stroke 27, 625–629.

Logg, A., Mardal, K.A., Wells, G.N., 2011. Automated Solution of Differential Equations by the Finite Element Method. Springer.

Miura, Y., Ishida, F., Umeda, Y., Tanemura, H., Suzuki, H., Matsushima, S., Shimosaka, S., Taki, W., 2013. Low wall shear stress is independently associated with the rupture status of middle cerebral artery aneurysms. Stroke 44, 519–521.

Rinkel, G.J.E., Djibuti, M., Algra, A., van Gijn, J., 1998. Prevalence and risk of rupture of intracranial aneurysms: a systematic review. Stroke 29, 251–256.

Robertson, A., Watton, P., 2012. Computational fluid dynamics in aneurysm research: critical reflections, future directions. American Journal of Neuroradiology 33, 992–995.

Robertson, A.M., Sequeira, A., Owense, R.G., 2009. Rheological models for blood. In: Formaggia, L., Quarteroni, A., Veneziani, A. (Eds.), Cardiovascular Mathematics. Modeling and Simulation of the Circulatory System. Springer-Verlag, Italia, Milano, pp. 211–241.

de Rooij, N., Linn, F., van der Plas, J., Algra, A., Rinkel, G.J.E., 2007. Incidence of subarachnoid haemorrhage: a systematic review with emphasis on region, age, gender and time trends. Journal of Neurology, Neurosurgery and Psychiatry 78, 1365–1372.

le Roux, A., Wallace, M., 2010. Outcome and cost of aneurysmal subarachnoid hemorrhage. Neurosurgery Clinics of North America 21, 235–246.

Schievink, W.I., 1997. Intracranial aneurysms. New England Journal of Medicine 336, 28–40.

Steinman, D.A., 2012. Assumptions in modelling of large artery hemodynamics. In: Modeling of Physiological Flows. Springer, pp. 1–18.

Valen-Sendstad, K., 2011. Computational Cerebral Hemodynamics. Ph.D. Thesis. University of Oslo.

Valen-Sendstad, K., Logg, A., Mardal, K.A., Narayanan, H., Mortensen, M., 2012a. A comparison of finite element schemes for the incompressible Navier–Stokes equations. In: Logg, A., Mardal, K.A., Wells, G.N. (Eds.), Automated Solution of Differential Equations by the Finite Element Method. Springer, pp. 399–420.

Valen-Sendstad, K., Mardal, K.A., Mortensen, M., Reif, B.A.P., Langtangen, H.P., 2011. Direct numerical simulation of transitional flow in a patient-specific intracranial aneurysm. Journal of Biomechanics 44, 2826–2832.

Valen-Sendstad, K., Mardal, K.A., Steinman, D.A., 2012b. High-resolution CFD detects high-frequency velocity fluctuations in bifurcation, but not sidewall, aneurysms of the middle cerebral artery. Journal of Biomechanics 46, 402–407.

Xiang, J., Natarajan, S.K., Tremmel, M., Ma, D., Mocco, J., Hopkins, L.N., Siddiqui, A., Levy, E.I., Meng, H., 2011. Hemodynamic-morphologic discriminants for intracranial aneurysm rupture. Stroke 42, 144–152.

Xiang, J., Tremmel, M., Kolega, J., Levy, E.I., Natarajan, S.K., Meng, H., 2012. Newtonian viscosity model could overestimate wall shear stress in intracranial aneurysm domes and underestimate rupture risk. Journal of Neurointerventional Surgery, 351–357.

Yeow, Y.L., Wickramasinghe, S.R., Leong, Y.K., Han, B., 2002. Model-independent relationships between hematocrit, blood viscosity, and yield stress derived from Couette viscometry data. Biotechnology Progress 18, 1068–1075.

Please cite this article as: Evju, Øyvind, et al., A study of wall shear stress in 12 aneurysms with respect to different viscosity models and flow conditions. Journal of Biomechanics (2013), http://dx.doi.org/10.1016/j.jbiomech.2013.09.004